A Robotic Aircraft that Follows Terrain Using a Neuromorphic Eye*

Thomas Netter[1], Nicolas Franceschini[2]

[1] *Laboratoire de Neurobiologie, CNRS, Marseille, France, tnetter@ini.unizh.ch*
[2] *Laboratoire de Neurobiologie, CNRS, Marseille, France, enfranceschini@lnb.cnrs-mrs.fr*

Abstract

Future Unmanned Air Vehicles (UAV) and Micro Air Vehicles (MAV) will fly in urban areas and very close to obstacles. We built a miniature (35 cm, 0.840 kg) electrically-powered aircraft which uses a motion-sensing visual system to follow terrain and avoid obstacles. Signals from the 20-photoreceptor onboard eye are processed by 19 custom Elementary Motion Detection (EMD) circuits which are derived from those of the fly. Visual, inertial, and rotor RPM signals from the aircraft are acquired by a flight computer which runs the Real-Time Linux operating system. Vision-guided trajectories and landings were simulated and automatic terrain-following flights at 2 m/s were demonstrated with the aircraft tethered to a whirling-arm. This UAV project is at the intersection of Neurobiology, Robotics, and Aerospace. It provides technologies for MAV operations.

1 Introduction

Robotic aircraft, or Unmanned Air Vehicles (UAV), are usually assigned to observation missions at altitudes higher than nearby terrain. Future missions will require small UAV, possibly Micro Air Vehicles (MAV), to fly in urban areas or very close to the ground and obstacles. Such missions require sensors and flight control methods for obstacle avoidance, terrain following and landing [8, 26, 30].

Flying insects use their wide Field of View (FOV) compound eyes to avoid obstacles and follow terrain. Insects use Optical Flow and fuse visual, inertial, and aerodynamic senses to control their flight [6, 7, 18].

This robotic UAV project uses biologically-inspired sensing in flight conditions that would daunt a remote-controlling operator. This *visuo-motor control* test bed demonstrates how insect vision can be applied to UAVs. This work continues a preliminary theoretical exploration on altitude control using Optical Flow (OF) [21] and is related to work inspired by insects [4, 14, 15, 23].

*Presented at IEEE/RSJ IROS 2002, paper 593, EPFL, Lausanne, Switzerland, Sep.30-Oct.4, http://iros02.epfl.ch

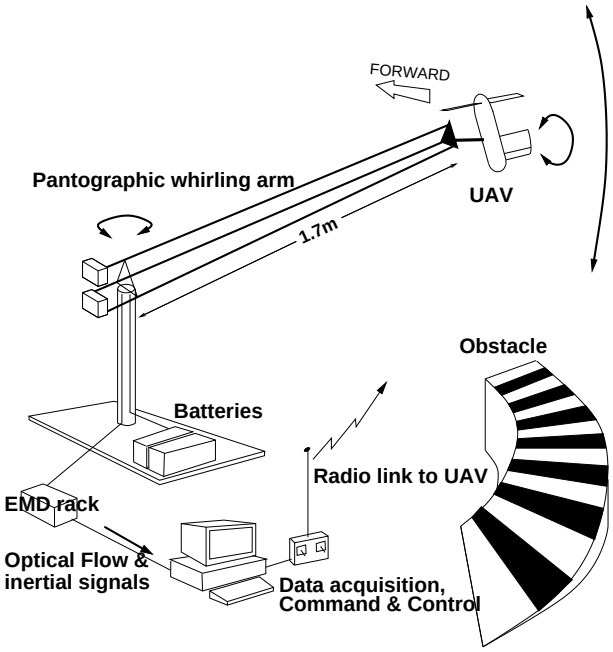

Figure 1: *Whirling-arm test bed.*

Section 2 summarizes how the aircraft is designed to eventually carry the entire sensory-motor system. Section 3 describes how we apply Optical Flow and its impact on sensor design. A simulation in section 4 shows how Optical Flow can be used to control flight. Section 5 presents the laboratory's indoors flight test bed (figure 1) and tests are reported in section 6.

2 Aircraft Design

The UAV is designed for low speed flight tests in a 4m × 4m area within the laboratory. This forbids large models such as helicopters or blimps. Small size and weight are needed to demonstrate the reactive maneuvers required for terrain following, obstacle avoidance, and hovering. The demonstrator is tethered to a whirling-arm so as to incrementally test the dynamics of a future autonomous aircraft.

The aircraft has a single rotor and uses Thrust Vectoring for Vertical Take-Off and Landing (VTOL)

and outstanding maneuvrability [11]. Recent UAV projects also explore this technology [5, 16, 20]. Our 3-degrees of freedom Proof of Concept aircraft features:

- A ⌀34 cm remote-controlled variable-pitch rotor that spins at 6000 RPM. The rotor is powered at 200W by a brushless motor. The rotor is based on model helicopter tail-rotor components and is sized to enable the aircraft to hover [24].
- A single remote-controlled vane immersed in the propeller flow. The actuated vane is sized to pitch the aircraft [29] and counter part of the rotor's torque on a future free-flying aircraft.

The aircraft weighs 0.84 kg. The three actuators (rotor speed, rotor blade pitch, vane angle) combined with visual and inertial sensing are used by the flight control system to vary thrust and aircraft pitch. This results in attitude, altitude, and speed control.

The future free-flying aircraft is envisioned as a compact ducted-rotor which provides high hovering thrust/weight for a given diameter and is safer to operate than a helicopter. Its axisymmetric configuration simplifies inertial characteristics and is a convenient shape for a 360° FOV eye and body-based behavior development.

3 Vision System

An artificial camera eye is easier and lighter to construct than a compound eye resembling that of an insect. A camera eye can be designed so that it is equivalent to a compound eye for the analysis of Optical Flow [10]. The camera eye contains a one-dimensional 20-pixel linear photoreceptor array and a plastic aspheric lens (focal length 24 mm) set at 13 mm from the array. The eye is tilted so that its FOV covers the forward and downward region (figure 2).

Biological visual systems rely on neural Elementary Motion Detectors (EMD) to compute the motion of contrast features projected onto the retina. Similarly to biological systems, the aircraft's photoreceptor array connects to an array of neuromorphic electronic EMDs derived from those of the fly [10]. Each EMD detects motion in a particular direction within the small part of the visual field seen by a pair of adjacent photoreceptors. When a contrasted edge passes in turn over the photoreceptors, filters in the first channel produce an exponentially decaying voltage whereas filters in the second channel produce a pulse. A multiplier combines both channels. The output of the EMD is a pulse whose voltage is nearly inversely proportional to the time delay between both photoreceptor excitations – hence quasi-proportional to speed. The EMD analog electronic circuits were developed for an earlier mobile robot project [9].

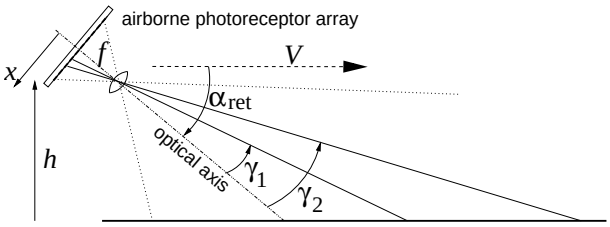

Figure 2: *Airborne eye with single lens and linear photoreceptor array moving at altitude h and horizontal speed V above ground.*

The retinal image is a quantized version of the visual environment [27]. The lens is mounted so as to defocus the retinal image. This deliberate blur (low-pass spatial filtering) reduces measurement errors due to aliasing [13]. Defocusing is estimated by measuring the Angular Sensitivity Function (ASF, characterized, e.g., by its angular width $\Delta\rho$ at half height) of a photoreceptor. The ASF is adapted to the sampling period (i.e., the interreceptor angle) $\Delta\varphi$ so that the Modulation Transfer Function (MTF) of the optical system is depressed beyond the Nyquist frequency $\eta = 1/(2\Delta\varphi)$.

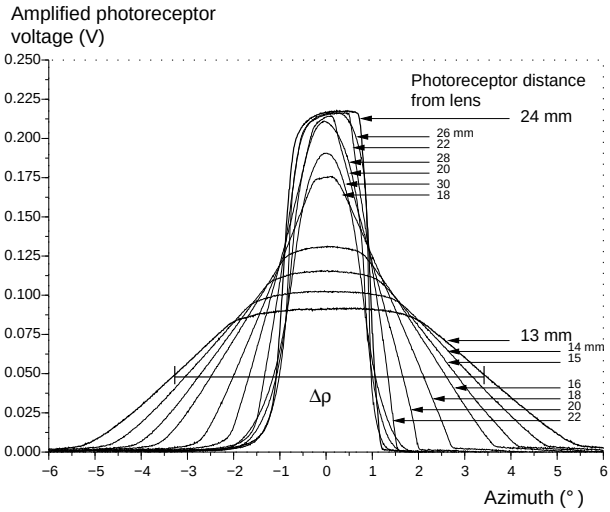

Figure 3: *The Angular Sensitivity Function (ASF) of a single photoreceptor (width 0.8mm) behind the eye lens is projected onto the photoreceptor array for 11 defocusing distances ranging from 13 to 30mm.*

We determined the ASF of the "lens-photoreceptor" system by translating a point light source across the FOV while measuring the voltage of a single photoreceptor. The ASF is measured for various lens-retina distances, i.e., various amounts of defocus (figure 3). A 13 mm defocus led to an adequate bell-shaped ASF with $\Delta\rho \approx 7°$, $\Delta\varphi \approx 4.2°$, and FOV $\approx 75°$.

4 Simulation of Terrain Following

Insects sometimes fly some pre-programmed maneuvers such as take-off with almost no visual feedback. In the simulation of terrain following the aircraft initially climbs with no visual feedback for a predefined time. The flight computer then reduces the thrust to a regime which corresponds approximately to horizontal flight. To a given attitude and thrust in undisturbed flight conditions corresponds a trajectory. The flight control system relies on predefined flight regimes obtained through experimental flight data interpolation. A steady thrust and attitude can be maintained through feedback from the tachymeter and inertial sensors. Manual flight tests (section 6) have shown that the aircraft can be left to fly hands-off even without this feedback.

When flying horizontally at altitude h and constant velocity V over a point on the horizontal ground (see [1] for a general description), the projected retinal velocity v_{ret} for a linear array is:

$$v_{\text{ret}} = -\frac{fV}{h}\frac{\sin^2(\alpha_{\text{ret}}+\gamma)}{\cos^2(\gamma)} \tag{1}$$

where f is the distance between optical center and retina, α_{ret} is the angle between the optical axis and V, γ is the angle between optical axis and photoreceptive pixel viewing axis. Equation (1) is plotted in figure 4. The forward part of the FOV generates nearly no Optical Flow and responds poorly to ground height variations, i.e., when the aircraft is approaching obstacles [12].

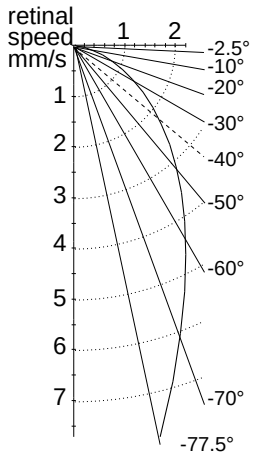

Figure 4: *Polar plot of equation (1) : retinal speed (mm/s) vs ray angle (deg) around the optical axis of the retina (α_{ret} = -40°, f = 13 mm, V = 2 m/s, h = 5 m).*

The altitude control regulator assumes the aircraft flies at initial pre-programmed altitude and groundspeed and that the terrain is flat. A corresponding reference OF distribution is calculated with equation (1). Terrain following is achieved by varying thrust by predefined increments so that the OF is adjusted to the reference OF. The pitch is stabilized to maintain horizontal airspeed.

Because the forward view is the most important for obstacle avoidance we devised a weighted average OF fusion scheme which gives more weight to the forward FOV than to the downward FOV. This paradigm is inspired by the response fields and dendritic structures of frontal neurons VS1 and VS2 of the blowfly's vertical vision system [17].

The reference Optical Flow which corresponds to the reference speed V_{ref} and altitude h_{ref} is fused into a reference weighted average:

$$\text{OF}_{\text{ref ave}} = \frac{1}{N}\sum_{i=1}^{N}\frac{\text{OF}_{\text{ref}N} - \text{OF}_{\text{ref}i}}{\text{OF}_{\text{ref}N}}\ \text{OF}_{\text{ref}i}\ , \tag{2}$$

where $i = 1$ is the most forward and $i = N$ the most downward viewing photoreceptor axis, respectively. A similar in-flight computation produces a current OF weighted average:

$$\text{OF}_{\text{ave}} = \frac{1}{N}\sum_{i=1}^{N}\frac{\text{OF}_{\text{ref}N} - \text{OF}_{\text{ref}i}}{\text{OF}_{\text{ref}N}}\ \text{OF}_{i} \tag{3}$$

It is then used to compute a ratio relating current and reference OF:

$$\text{OF}_{\text{ratio}} = \frac{\text{OF}_{\text{ref ave}} - \text{OF}_{\text{ave}}}{\text{OF}_{\text{ref}N}} \tag{4}$$

Noticing that OF variation is inversely proportional to the square of altitude

$$\frac{dv_{\text{ret}}}{dh} = \frac{fV}{h^2}\frac{\sin^2(\alpha_{\text{ret}}+\gamma)}{\cos^2(\gamma)}\ , \tag{5}$$

we produce a request for a new altitude:

$$h_{\text{req}} = h - h_{\text{ref}}\ \text{sign}(\text{OF}_{\text{ratio}})\sqrt{|\text{OF}_{\text{ratio}}|}\ . \tag{6}$$

The terrain following simulation was programmed with Scilab [25]. Figure 5(a) depicts the path of the aircraft eye's optical center over terrain with the 20 photoreceptor viewing axes. It shows that terrain can be followed with a low number of pixels if moving contrasts are detected. Furthermore, the initial flight phase illustrates that steep obstacles can be overcome providing adequate initial altitude and flight speed for a given forward FOV setting.

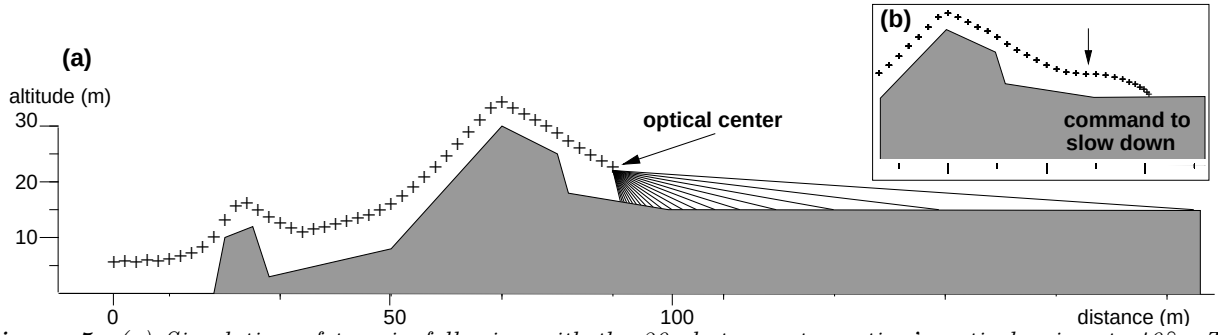

Figure 5: *(a) Simulation of terrain following with the 20-photoreceptor retina's optical axis set -40°. The FOV is 75° in the vertical plane, i.e., within the lens's physical limits. V = 2 m/s, h_{init} = 5 m, iteration step = 1 s. (b) An automatic landing was simulated by linearly decreasing the aircraft horizontal speed by 10% of the initial reference speed at every iteration while retaining the same request to maintain a reference OF condition.*

A landing is simulated by linearly decreasing the aircraft's horizontal speed by 10% of the initial reference speed at every iteration while maintaining the reference OF (figure 5(b)). Bees, however, decrease their speed exponentially and descend at constant angle [28]. Whether bee, flying locust, or bio-inspired flying robot, a decrease in horizontal flight speed results in a decrease in altitude so as to maintain optical flow.

5 Experimental Rig

The pantographic whirling-arm rig (figure 1) built for the flight tests is a modern version of John Smeaton's 1759 apparatus built for aerodynamic studies of windmills [2]. The arm is 1.7m in radius (steel base and pole, carbon fiber arm). It prevents yaw and roll of the UAV and limits pitch (±30°) and altitude (0.5 to 2.5 m). The arm's elevation and azimuth are measured by a potentiometer and an optical encoder, respectively. These measurements are used for experiment recording only, not for flight control.

The rotorcraft (figure 6) is powered at 24V, 8A, by two car batteries at the base of the arm. Current is fed to the aircraft through heavy duty bearings. Visual, inclinometer, and tachymeter RPM signals are transmitted from the UAV to the rig's base through a slip-ring assembly. The 20 photoreceptor signals are pre-amplified onboard and fed to 19 EMD printed-circuit boards which are digitized by a National Instruments 64-inputs acquisition board. The PC runs the Real-Time Linux [3] operating system. Flight commands are output at 20 Hz via the parallel port to a microcontroller interface which generates a Pulse Width Modulated (PWM) signal compatible with a standard radio-control model transmitter. The onboard receiver dispatches the 3 flight commands to the rotor speed variator, the collective pitch, and vane servos. The aircraft can be piloted manually.

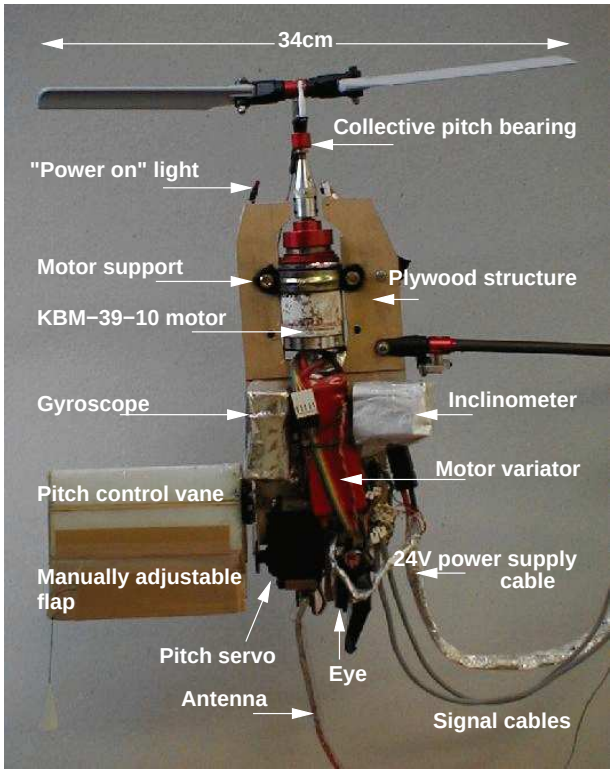

Figure 6: *The visually-guided Fania rotorcraft weighs 0.84 kg (front view).*

6 Flight Tests

The whirling arm was used for piloted [22] and automatic terrain following flight tests.
Like helicopters, the aircraft has two noticeable flight regimes: low speed and cruise. Thrust is increased by either increasing rotor RPM or increasing collective pitch. It is possible to stall the rotor. It is easy to pilot either small or suddenly large rates of climb using collective pitch. Strong action on the blown vane can reverse the flight aggressively thanks

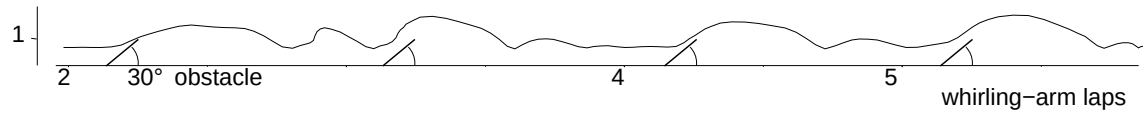

Figure 8: *Altitude versus whirling-arm laps for a few visually-guided leaps. The oblique bars represent the obstacle ramp and indicate its position and extension (height in meters, slope ≈ 30°) at each lap.*

to thrust vectoring. The aircraft can be flown at 6 m/s but at that speed centrifugal forces tend to force the whirling-arm to remain horizontal. Some speed and vane configurations can lead to oscillations due to the vane being alternatively immersed in rotor or stalling in free-stream airflow. Low speed and hovering are easy to pilot after some practice. Piloted flights were used to identify the rotorcraft's response to vane inputs and to elaborate a PID-based pitch regulator (figure 7).

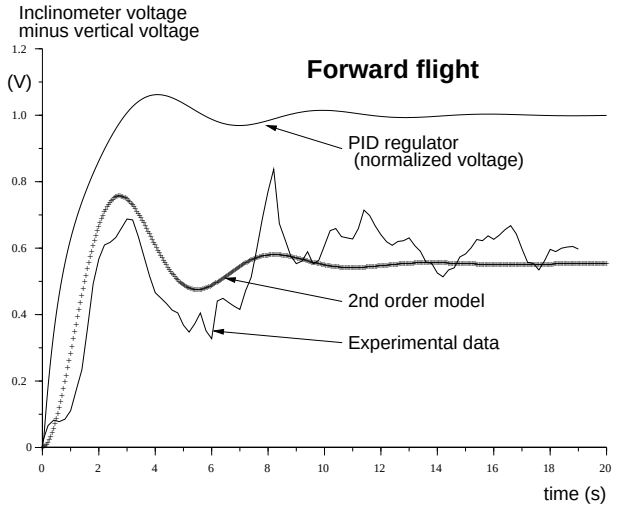

Figure 7: *Experimental data fitted with a second-order model of the pitch response to a 60% step deflection (+28°) of the elevator vane for forward flight. Experimental data is digitized at 20 Hz and smoothed over 5 samples. The top curve plots the normalized pitch response to a step input following PID tuning (sample rate = 20 Hz) of the second-order model.*

The aircraft flew more than 50 automatic terrain following and obstacle avoidance flight tests. A flight sequence starts with a rotor spool-up followed by a pre-programmed collective pitch increase that induces take-off. The aircraft then loiters a few seconds and descends until terrain bearing contrasted features stimulates the retina. Flight continues for a preset time during which 4 obstacle avoidance events occur (figure 8). The obstacle is an arc of length 2.25 m and width 0.5 m with 10 black paper bands (width = 10 cm) that are taped at regular intervals of 10 cm on a white background. This planar obstacle produces a 30° ramp whose peak is at 1.5 m. The collective pitch, hence the lift, is incremented by discrete steps as a function of the fused signal from the EMDs. When no contrasts are visible the collective pitch is reduced. The rotor's thrust introduces some ground effect. At the end of the experiment an audible signal warns the experimenter to lower the obstacle ramp and the motor RPM is automatically reduced until the aircraft reaches the lowest height permitted by the whirling-arm.

7 Conclusion

This paper described the design, construction, and initial flight tests of a miniature robotic aircraft on a whirling-arm test bed. The aircraft is original because it demonstrates:

- Visually controlled reactive maneuvers,
- An analogue electronic vision system, inspired from biology, to avoid obstacles during flight and follow terrain,
- Thrust-vectoring technology for reactive maneuvres,
- The Real-Time Linux operating system for flight control.

The project is multidisciplinary and combines concepts from the fields of Neurobiology, Aerodynamics, Optics, Electronics, Vision, and Automatic Control. The aircraft is designed as a single rotor aircraft with an aerodynamic vane for pitch control which enables it to hover or fly at low speed. By adding vanes and a rotor shroud the design can be generalized to become a free-flying aircraft. The vision system is based on a 20-photoreceptor linear array. The signals from the photoreceptors are processed by 19 analog electronic Elementary Motion Detectors inspired from biology. The flight computer fuses the digitized EMD signals with a weighted averaging paradigm which gives most importance to motion in the frontal FOV. Simulations and flight tests show that the same visual flight control paradigm can be used for terrain following and automatic landing.
This project helps understand how insects can control their flight with a low number of pixels. It also reproduces the altitude control behavior which is observed in many insects. Because only few pixels are needed for flight control this technology is interesting for vehicles with very limited processing power

such as Micro Air Vehicles (MAV). The paradigm offers an alternative to high-precision computer vision techniques [19]. The next step is to implement the visual flight control system on a chip, possibly using analog VLSI technology.

Acknowledgments

We thank Marc Boyron and Jean Roumieu for their expertise in electronics and precision mechanics, respectively. Thomas Netter was supported by a CogniSciences doctoral stipend of the French Ministry of Education and Research. This research is supported by the CNRS (Life Science, Engineering Science, Cogniscience, and Microsystems program) and by EC contracts (TMR and IST/FET).

References

[1] J.S. Albus and T. Hong Hong. Motion, depth, and image flow. In *Proceedings of the 1990 IEEE Int. Conf. on Robotics and Autom.*, pages 1161–1170, 1990.

[2] John D. Anderson. *A History of Aerodynamics*. Cambridge University Press, Cambridge, UK, 1997.

[3] M. Barabanov and V. Yodaiken. www.rtlinux.org.

[4] G. Barrows and C. Neely. Mixed-mode VLSI optic flow sensors for in-flight control of a micro air vehicle. *Proc. SPIE*, 4109:52–63, 2000.

[5] K. M. Black, J. O. Smith, and R. A. Roberts. The UTA autonomous aerial vehicle - automatic control and navigation. In *Nat. Aero. and Elec. Conf.*, 1992.

[6] Erich Buchner. Behavioural analysis of spatial vision in insects. In M. A. Ali, editor, *Photoreception and vision in arthropods*, pages 561–621. Plenum, 1984.

[7] Wai Pang Chan, Frederick Prete, and Michael H. Dickinson. Visual input to the efferent control system of a fly's "gyroscope". *Science*, 280:289–292, 1998.

[8] V. H.L. Cheng and B. Sridhar. Technologies for automating rotorcraft Nap-of-the-Earth flight. *J. American Helicopter Society*, pages 78–87, April 1993.

[9] Nicolas Franceschini, Jean-Marc Pichon, and Christian Blanes. From insect vision to robot vision. *Phil. Trans. R. Soc. B*, 337:283–294, 1992.

[10] Nicolas Franceschini, Alexa Riehle, and Agnes Le Nestour. Directionally selective motion detection by insect neurons. In *Facets of Vision*, chapter 17, pages 360–390. Springer-Verlag, Berlin, 1989.

[11] B. Gal-Or. *Vectored Propulsion, Supermaneuvrability, and Robot Aircraft*. Springer-Verlag NY, 1990.

[12] James G. Gibson, Paul Olum, and Frank Rosenblatt. Parallax and perspective during aircraft landings. *Amer. J. Psychology*, 68:372–385, 1955.

[13] K.G. Götz. Die optischen Übertragungseigenschaften der Komplexaugen von Drosophila. *Kybernetik*, 2:215–221, 1965.

[14] Fumiya Iida. Goal-directed navigation of an autonomous flying robot using biologically inspired cheap vision. In *32nd Int. Symp. on Robotics*, pages 1404–1409, Seoul, Korea, 2001.

[15] Fumiya Iida and Dimitrios Lambrinos. Navigation in an autonomous flying robot by using a biologically inspired visual odometer. In *SPIE Photonics East, Boston, MA*, volume 4196, pages 86–97. SPIE, Bellingham, WA, 2000.

[16] Michael Kantner, Bobby Bodenheimer, Pascale Bendotti, and Richard M. Murray. An experimental comparison of controllers for a vectored thrust, ducted fan engine. In *American Control Conference*, Seattle, WA, 1995. IEEE Control Systems Society.

[17] Holger G. Krapp, Bärbel Hengstenberg, and Roland Hengstenberg. Dendritic structure and receptive-field organization of optic flow processing interneurons in the fly. *Journal of Neurophysiology*, 79(4):1902–1917, April 1998.

[18] Myriam Lehrer, Mandyam V. Srinivasan, Shao-Wu Zhang, and George Adrian Horridge. Motion cues provide the bee's visual world with a third dimension. *Nature*, 332:356–357, 1988.

[19] J.R. Miller, O. Amidi, C. Thorpe, and T. Kanade. Precision 3-D modeling for autonomous helicopter flight. In *Int. Symp. Robotics Research (ISRR)*, pages 147–152, Snowbird, UT, 1999.

[20] Stephen Morris. Design and flight test results for micro-sized fixed-wing and VTOL aircraft. In *The First International Conference on Emerging Technologies for Micro Air Vehicles*, Atlanta, GA, 1997.

[21] Fabrizio Mura and Nicolas Franceschini. Visual control of altitude and speed in a flying agent. In D. Cliff et al., editor, *From Animals to Animats III*, pages 91–99. MIT Press, 1994.

[22] Thomas Netter and Nicolas Franceschini. Neuromorphic optical flow sensing for nap-of-the-earth flight. In *SPIE Conference on Mobile Robots XIV*, volume 3838, pages 208–216, Boston, MA, Sep. 19-22 1999.

[23] Titus R. Neumann and Heinrich H. Bülthoff. Insect inspired visual control of translatory flight. In *ECAL 2001*, pages 627–636. Springer-Verlag, 2001.

[24] Raymond W. Prouty. *Helicopter Performance, Stability, and Control*. Krieger, Malabar, FL, 1995.

[25] Scilab Group. http://www-rocq.inria.fr/scilab/.

[26] Omid Shakernia, Yi Ma, John Koo, and Shankar S. Sastry. Landing an unmanned aerial vehicle: Vision based motion estimation and nonlinear control. *Asian Journal of Control*, 1(3):128–145, 1999.

[27] Allan W. Snyder. Acuity of compound eyes: physical limitations and design. *J. Comp. Physiol.*, pages 161–182, 1977.

[28] Mandyam V. Srinivasan, S. W. Zhang, J. S. Chahl, E. Barth, and S. Venkatesh. How honeybees make grazing landings on flat surfaces. *Biological Cybernetics*, 83:171–183, 2000.

[29] D. Stinton. *The Design of the Aeroplane*. BSP Professional Publishing, Oxford, UK, 1983.

[30] M. Williams, D.I. Jones, and G.K. Earp. Obstacle avoidance during aerial inspection of power lines. *Aircraft Engineering and Aerospace Technology*, 73(5):472–479, 2001.